https://doi.org/10.5194/egusphere-2025-6033
Preprint. Discussion started: 15 January 2026

Indirect climate forcing from ozone depleting substances

William J. Collins[1], John S. Daniel[2], Martyn P. Chipperfield[3,4], Martin Cussac[5], Makoto Deushi[6], Gregory Faluvegi[7,8], Paul Griffiths[9], Øivind Hodnebrog[10], Larry W. Horowitz[11], James Keeble[12], Douglas Kinnison[13], Vaishali Naik[11], Fiona M. O'Connor[14,15], Drew Shindell[16], Simone Tilmes[13], Kostas Tsigaridis[7,8], Zihao Wang[3], James Weber[1]

[1] Department of Meteorology, University of Reading, Reading, RG6 6BB, UK
[2] NOAA Chemical Sciences Laboratory, Boulder, CO 80305, USA
[3] School of Earth and Environment, University of Leeds, Leeds, LS2 9JT, UK
[4] National Centre for Earth Observation, University of Leeds, Leeds, LS2 9JT, UK
[5] Météo-France, CNRS, Univ. Toulouse, CNRM, Toulouse, France.
[6] Meteorological Research Institute, Japan Meteorological Agency, Tsukuba, Japan
[7] Center for Climate Systems Research, Columbia University, Palisades, NY, 10964, USA
[8] NASA Goddard Institute for Space Studies, Palisades, NY, 10964, USA
[9] School of Chemistry, University of Bristol, Bristol, United Kingdom
[10] CICERO Center for International Climate Research, Oslo, Norway
[11] NOAA Geophysical Fluid Dynamics Laboratory, Princeton, NJ, 08540, USA
[12] Lancaster Environment Centre, Lancaster University, Lancaster, UK
[13] Atmospheric Chemistry Observations & Modeling Laboratory, NSF National Center for Atmospheric Research, Boulder, CO 80307, USA
[14] Met Office Hadley Centre, Exeter, United Kingdom
[15] Department of Mathematics & Statistics, Global Systems Institute, University of Exeter, Exeter, United Kingdom
[16] Nicholas School of the Environment, Duke University, Durham, NC, 27708, USA

Correspondence to: Bill Collins (w.collins@reading.ac.uk)

Abstract

Many halocarbons are powerful greenhouse gases and also influence climate indirectly through depletion of stratospheric ozone which opposes their direct greenhouse effect. Changes in effective radiative forcing (ERF) from historical ozone depletion have been diagnosed from model experiments with perturbed halocarbons run under the sixth Coupled Model Intercomparison Project. This is more negative than the offline stratospheric-temperature-adjusted radiative forcing (SARF). Including effects of ozone depletion on the methane lifetime makes the historical net ERF of ozone depleting substances consistent with zero. The Integrated Ozone Depletion (IOD) metric has been used to apportion this ERF between the halocarbon species and thereby derive indirect 100-year Global Warming Potentials (GWP100s) for a suite of halocarbons. The indirect GWP100 for CFC-11 is enough to make the net GWP100 likely negative, whereas the indirect contribution for CFC-12 is smaller due to a combination of longer stratospheric lifetime and fewer chlorine atoms. Thus for CFC-12 the net GWP100 is positive, but reduced by 38%. The use of the online ERF, rather than the offline SARF, allows the model physics to account for changes in stratospheric temperature (as well as tropospheric temperature, water vapour and clouds) rather than

https://doi.org/10.5194/egusphere-2025-6033
Preprint. Discussion started: 15 January 2026

estimating stratosphere temperature changes using fixed dynamical heating. This online calculation of radiative forcing rather than offline leads to approximately double the indirect GWPs compared to World Meteorological Organization assessments. This formalism can be used with other estimates of ozone ERF, as the indirect GWPs scale linearly with this quantity.

Short Summary

Ozone depleting substances (ODSs) are also greenhouse gases that cause global warming. However, their destruction of ozone contributes a global cooling. We have used results from climate models that include atmospheric chemistry and found that the cooling effect of the ozone depletion diagnosed in the models was larger than that calculated using a standard method. We find that some ODSs have a net cooling effect whereas for others the warming effect is significantly reduced.

1 Introduction

Ozone depleting substances (ODSs) such as chlorofluorocarbons (CFCs) and hydrochlorofluorocarbons (HCFCs) are typically radiatively active in the thermal infrared and hence they act as greenhouse gases. The wider category of halocarbons also includes hydrofluorocarbons (HFCs) and perfluorocarbons (PFCs) which also act as greenhouse gases, but do not deplete ozone. In this study we focus on the subset of halocarbons that do deplete ozone. The Intergovernmental Panel on Climate Change 6th assessment report (IPCC AR6) concluded that increases in ODSs (sum of CFCs + HCFCs + other ozone depleting substances covered by the Montreal Protocol) have caused an effective radiative forcing (ERF) of 0.354 Wm^{-2} over the period 1750-2019 (Forster et al., 2021). These headline values only considered the direct greenhouse effect and any adjustments to meteorology. Indirect contributions to the ODS radiative forcing from their chemical effects, were assessed in a separate chapter (Szopa et al., 2021).

The chemical effects of ODSs come principally through depleting ozone in the stratosphere contributing negative radiative forcings. The depletion of ozone also allows more UV radiation to penetrate to the troposphere, increasing the production of OH and reducing the lifetime of methane, which also contributes to negative radiative forcing. The increase in tropospheric OH following stratospheric ozone depletion can also favour the gas-phase oxidation route of SO_2 compared to the aqueous-phase route (O'Connor et al., 2022). This can increase new particle formation and so enhance (negative) ERF from aerosol-cloud interactions (Toumi et al., 1994). The decay products from halocarbons can also cause a small warming of a few percent of the direct effect (Thornhill et al., 2024).

The earlier estimates of the radiative forcing due to stratospheric ozone depletion came from observations of stratospheric ozone change (Forster et al., 2007; Ramaswamy, 2001; Ramaswamy et al., 1992). Although the observation periods were chosen such that the expected contributions to the ozone change came mainly from ODSs, these periods will have included

https://doi.org/10.5194/egusphere-2025-6033
Preprint. Discussion started: 15 January 2026

the impacts of changes in other factors, such as temperature, circulation, water vapour, tropospheric ozone precursors, and N_2O. For the AR5 and AR6 IPCC reports (Myhre et al., 2013; Szopa et al., 2021), the radiative forcing from stratospheric ozone changes was specifically based on Earth system model (ESM) simulations where only halocarbons change. If the models represent the ozone depletion realistically these are more likely to be directly applicable to understanding the indirect radiative forcing contribution of halocarbons since they do not conflate the contributions of meteorological changes (other than responses to ozone) and N_2O. Additionally, models account for tropospheric ozone changes in response to stratospheric depletion due to increased penetration of UV radiation and exchange of air between the stratosphere and troposphere; upper tropospheric ozone, in particular, has a strong radiative signature (Shindell et al., 2013a) .

IPCC AR6 assessed that effects on ozone, methane and aerosols (including aerosol-cloud interactions) from increases in halocarbons over the 1750-2019 period contributed -0.162, -0.051, and -0.025 Wm^{-2}, respectively, to the historical ODS ERF (Szopa et al., 2021), i.e. offsetting over 60% of the direct ERF. This IPCC assessment was largely based on analysis of ESM experiments (Thornhill et al., 2021b) carried out using the Coupled Model Intercomparison Project 6 (CMIP6) Aerosols and Chemistry Model Intercomparison Project (AerChemMIP) protocol (Collins et al., 2017).

The ozone adjustments in Thornhill et al. (2021b) were calculated using an offline stratospheric-temperature-adjusted radiative forcing (SARF) which uses fixed dynamical heating to estimate the stratospheric-temperature adjustment (Fels et al., 1980). The ERF from ODSs was calculated by Morgenstern et al. (2021). Their ERF is determined internally in the models and implicitly includes the stratospheric-temperature adjustment (as well adjustments from tropospheric temperature, water vapour and clouds) from changes in meteorological fields within the model. Morgenstern et al. (2021) calculated an ERF due to ozone depletion of -0.326 Wm^{-2} (subtracting their "discounting ozone depletion" ERF from their total). This ozone depletion ERF includes the radiative effects of changes to ozone and aerosols. It largely excludes the effects on methane lifetime since surface methane concentrations were fixed, hence this ERF value can be compared to the offline SARF value (ozone + aerosols) of -0.187 Wm^{-2} in Szopa et al. (2021). A comparison of ERF and offline SARF in Collins et al. (2025) also finds the ERF from ozone depletion is approximately double the offline SARF.

The above analyses did not attribute the ozone depletion ERFs to individual halocarbon species, but rather to baskets of halocarbons, with each modelling centre using different baskets depending on the set up of their chemistry schemes. The World Meteorological Organization (WMO) Scientific Assessments of Ozone Depletion (WMO 1994 and onwards) have used a methodology based on Daniel et al. (1995) which relates changes in the radiative forcing of stratospheric ozone to changes in Equivalent Effective Stratospheric Chlorine (EESC). Forcing contributions of individual species can be then estimated from their contribution to EESC. An alternative to EESC for attributing ozone depletion to different species is the recently proposed Integrated Ozone Depletion (IOD) (Pyle et al., 2022). EESC and IOD will be discussed further in Section 2.

https://doi.org/10.5194/egusphere-2025-6033
Preprint. Discussion started: 15 January 2026

The aim of this paper is to show how EESC and IOD can be used to attribute the historical ODS total effective radiative forcing to the individual halocarbons and use these to quantify emission climate metrics such as net global warming potential (GWP).

2 Theoretical framework

The amount of ozone depleted from a halocarbon species is expected to be related to the number of chlorine and bromine atoms released in the stratosphere. Two metrics are available for this, the IOD and EESC which are discussed below.

2.1 Integrated ozone depletion

The IOD (Pyle et al., 2022) is an integrated measure of ozone depletion for a pulse emission of a long-lived ODS. It determines the total amount of equivalent chlorine released using the fraction of the ODS degradation that occurs in the stratosphere. This fraction is calculated using the ratio of the total species lifetime τ to stratospheric lifetime τ_{strat}, where τ and τ_{strat} are defined as the total atmospheric burden divided by the total loss rate and stratospheric loss rate respectively.

$$\text{IOD} = K \times (n_{\text{Cl}} + \alpha n_{\text{Br}}) \times \left(\frac{\tau}{\tau_{\text{strat}}}\right) \times \frac{m_{\text{Cl}}}{m} \times E; \quad \text{Equation 1}$$

Where, E is the mass of halocarbon emitted (in Tg), m is the molar mass of the species, m_{Cl} is the molar mass of chlorine and K is a constant of proportionality; n_{Cl}, n_{Br} are the number of chlorine and bromine atoms in the molecule respectively, α is the relative efficiency factor for bromine. IOD has the units of Dobson Units × years (DU yr) and quantifies the integral over all time of the ozone depleted by the halocarbon following its emission. The units of K are therefore DU yr Tg(Cl)$^{-1}$, and the units of the remainder of the right-hand side of Equation 1, (i.e. $(n_{\text{Cl}} + \alpha n_{\text{Br}}) \times \left(\frac{\tau}{\tau_{\text{strat}}}\right) \times \frac{m_{\text{Cl}}}{m} \times E$), are Tg(Cl) and hence a measure of total equivalent chlorine production.

Since IOD is an integrated measure, this can easily be converted to an absolute global warming potential with infinite time horizon ($\text{AGWP}_{\infty} = -\text{IOD} \times \phi_{O_3}/E$) if we assume a fixed radiative efficiency of stratospheric ozone changes ϕ_{O_3} in Wm^{-2} DU^{-1} that is independent of the halocarbon causing the depletion. AGWPs at finite time horizons H can be calculated assuming an exponential decay of the halocarbon and its ozone response: $\text{AGWP}_H = \text{AGWP}_{\infty} \left(1 - e^{-H/\tau}\right)$. The indirect GWPs from halocarbons due to their ozone depletion can therefore be calculated by dividing by the corresponding AGWP for CO_2.

While Pyle et al. (2022) used experiments with pulse emissions to derive K, many model experiments e.g. Thornhill et al. (2021b) have used specified concentrations rather than emission pulses. These are useful to derive ϕ_{O_3}. However, these can also be used in the IOD framework since the integral of the response to a pulse emission is equal to the instantaneous response to a continuous emission change (Equations S1-S2); hence we can also write:

$$\text{OD}_{\infty} = K \times (n_{\text{Cl}} + \alpha n_{\text{Br}}) \times \left(\frac{\tau}{\tau_{\text{strat}}}\right) \times \frac{m_{\text{Cl}}}{m} \times e; \quad \text{Equation 2}$$

https://doi.org/10.5194/egusphere-2025-6033
Preprint. Discussion started: 15 January 2026

Where OD_∞ is now the ozone depletion (in DU) at equilibrium ($H \to \infty$) and e is now the rate of constant continuous emission of a halocarbon (in Tg yr^{-1}). All other terms are as in Equation 1. The OD_∞ (in DU) for a 1 kg yr^{-1} emission increase is therefore numerically equal to the IOD (in DU yr) for a 1 kg pulse emission.

The rate of emission needed to achieve surface concentration C is:

$$e = \frac{1}{\tau} \times \frac{m}{m_{\text{air}}} \times M_{\text{atm}} \times \frac{\bar{C}}{C}; \text{ Equation 3}$$

where m_{air} is the molar mass of air and M_{atm} is the mass of the atmosphere. The factor $\frac{\bar{C}}{C}$ is the ratio of the atmospheric average concentration to surface concentration (Volk et al., 1997) and is referred to as "fill factor" in Prather et al. (2012). It accounts for the decline in concentration with altitude in the stratosphere and is species dependent. Hence Equation 2 can be rewritten:

$$OD_\infty = K \times (n_{\text{Cl}} + \alpha n_{\text{Br}}) \times \left(\frac{1}{\tau_{\text{strat}}}\right) \times C \times \frac{m_{\text{Cl}}}{m_{\text{air}}} \times M_{\text{atm}} \times \frac{\bar{C}}{C}; \text{ Equation 4}$$

Equation 4 can therefore be used to determine K, IOD and GWPs from experiments with step changes in concentration run to equilibrium.

2.2 Comparisons with ODP and EESC

The IOD is related to the semi-empirical ozone depletion potential (ODP) (Pyle et al., 2022):

$$ODP = (n_{\text{Cl}} + \alpha n_{\text{Br}}) \times f \frac{\tau}{m} / \left(\frac{3\tau_{\text{CFC11}}}{m_{\text{CFC11}}}\right); \text{ Equation 5}$$

where f is the fractional release, i.e. the fraction of halocarbon oxidised in the stratosphere at any time (Daniel et al., 1995).

Hence $$\frac{IOD}{E \times K} = ODP \times \left(\frac{1}{\tau_{\text{strat}} \times f}\right) \times m_{\text{Cl}} \left(\frac{3\tau_{\text{CFC11}}}{m_{\text{CFC11}}}\right); \text{ Equation 6}$$

Therefore, IOD is proportional to ODP if f is proportional to $\left(\frac{1}{\tau_{\text{strat}}}\right)$. Figure 1 uses values of extra-polar f and τ_{strat} from Tables 7-2 and A5 in WMO (2022) and shows that this proportionality does approximately hold with a slope of roughly 25 yr.

https://doi.org/10.5194/egusphere-2025-6033
Preprint. Discussion started: 15 January 2026

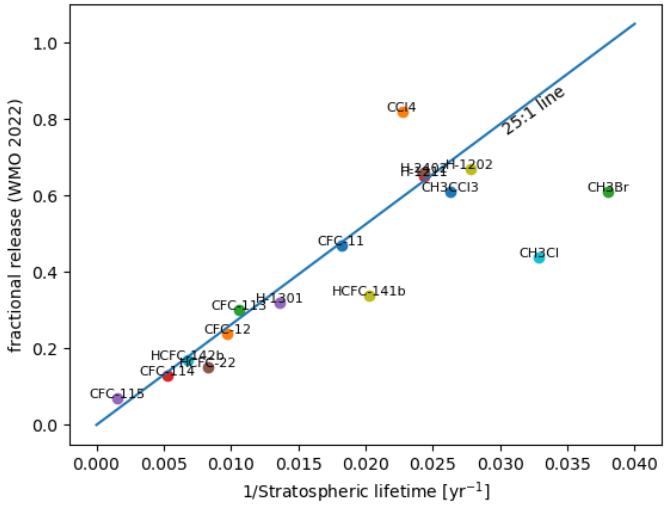

Figure 1 extra-polar fractional release f against 1/stratospheric lifetime τ_{strat} for species in WMO (2022). **Also shown is the 25:1 yr line.**

The EESC also uses the fractional release f (Daniel et al., 1995).

$$\mathrm{EESC(t)} = (n_{\mathrm{Cl}} + \alpha n_{\mathrm{Br}}) \times f \times C^{t-3}; \qquad \text{Equation 7}$$

where C^{t-3} is the concentration of the species at the surface 3 years previously. EESC can be split into polar and extra-polar components which have different values for f and α; the time lag for polar chlorine is taken to be 5.5 years (Newman et al., 2007). EESC(t) is an instantaneous measure of equivalent stratospheric chlorine at any time point t and has units of concentration of Cl, usually reported in parts per trillion – ppt(Cl). It is assumed that the halocarbon contribution to ozone depletion (polar or extra-polar) in any year is proportional to the (polar or extra-polar) EESC in that year, where the constant of proportionality can differ between polar and extra-polar regions.

Comparing Equations 4 and 7 for constant concentrations, OD_{∞} (the concentration-based form of the IOD) can be related to the EESC.

$$\frac{\mathrm{OD}_{\infty}}{K} = EESC \times \left(\frac{1}{\tau_{\mathrm{strat}} \times f}\right) \times \frac{m_{\mathrm{Cl}}}{m_{\mathrm{air}}} \times M_{\mathrm{atm}} \times \frac{\bar{C}}{C}; \text{ Equation 8}$$

So OD_{∞} and EESC are also approximately proportional since f is approximately proportional to $\left(\frac{1}{\tau_{\mathrm{strat}}}\right)$.

https://doi.org/10.5194/egusphere-2025-6033
Preprint. Discussion started: 15 January 2026

3 Methodology

3.1 Experimental design

The models used in this analysis participated in the CMIP6 AerChemMIP project (Collins et al., 2017). The experiments used were *piClim-control* and *piClim-HC*. In *piClim-control* well-mixed greenhouse gases and emissions of short-lived species are fixed at 1850 levels, sea surface temperatures and sea ice are prescribed as a (monthly varying) climatology taken from 30 years of the pre-industrial control experiment (*piControl*) (Eyring et al., 2016). In *piClim-HC* the protocol was to increase halocarbons (ODSs and non-ODSs) to 2014 levels (Meinshausen et al., 2017). Both experiments were run as time slices, i.e. with fixed conditions for at least 30 years. Individual modelling centres had different implementations of halocarbon chemistry and so followed different procedures when increasing halocarbon concentrations for *piClim-HC*. Models differed according to whether they specified halocarbon concentrations as a fixed value throughout the atmosphere (GFDL-ESM4, , MRI-ESM2) or whether they specified surface concentrations and allowed the model advection and chemistry to determine the concentrations away from the surface (CESM2-WACCM, CNRM-ESM2-1, GISS-E2-1-G, UKESM1-0-LL). Note for *piClim-HC* in models that specified concentration changes at the surface it took a few years for the changes to reach the stratosphere except for GISS-E2-1-G where the concentrations are initialised to the expected values throughout the atmosphere. Results are taken as the mean of the last 30 years of the simulations. The 2014 concentrations of halogenated species used in the different models is shown in Table S1.

3.2 Model implementation of aerosols, tropospheric and stratospheric chemistry

3.2.1 CESM2-WACCM

The Whole Atmosphere Community Climate Model version 6 (WACCM6) is a version of the Community Atmosphere Model, version 6 (CAM6), (Danabasoglu et al., 2020; Gettelman et al., 2019). The model has 70 levels with a vertical range from the surface to the lower thermosphere. The vertical resolution in the lower stratosphere ranges from 1.2 km near the tropopause to ~2 km near the stratopause.

The baseline chemical mechanism (the collection of reactions and species) contains reactions relevant for the whole atmosphere: troposphere, stratosphere, mesosphere and lower thermosphere. The chemical species within this mechanism include the extended Ox, NOx, HOx, ClOx, and BrOx chemical families, along with CH_4, N_2O, H_2O, plus various natural and anthropogenic precursors of the ClOx and BrOx families (Emmons et al., 2020; Gettelman et al., 2019; Tilmes et al., 2019). The WACCM mechanism includes a total of 231 solution species, 583 chemical reactions broken down into 150 photolysis reactions, 403 gas-phase reactions, 13 tropospheric, and 17 stratospheric heterogeneous reactions. The photolytic calculations are based on both inline chemical modules and a lookup table approach (Kinnison et al., 2007). The chemical mechanism

https://doi.org/10.5194/egusphere-2025-6033
Preprint. Discussion started: 15 January 2026

includes two very short-lived halogens: $CHBr_3$ and CH_2Br_2. The surface mole fraction for these two species is set to 1.2 pptv (i.e., 6 pptv of total bromine). This approach adds an additional ~5 pptv of inorganic bromine to the stratosphere. The heterogeneous reactions use aerosol surface area density (SAD) derived from MAM4 (Mills et al., 2016). The stratosphere heterogeneous reactions occur on three aerosol types (i.e., sulphate, nitric acid trihydrate, and water-ice) (Solomon et al., 2015).

3.2.2 CNRM ESM2-1

The CNRM-ESM2-1 model (Michou et al., 2020; Séférian et al., 2019) includes an interactive gaseous chemistry scheme only above the level of 560 hPa. It includes the REPROBUS-C_v2 chemistry scheme which includes 168 chemical reactions and has explicit treatment of 7 chlorinated and 3 brominated species (Michou et al., 2011). The chemical scheme considered several family species, among which more specifically for halogens, the ClOx, BrOx, Bry, and Cly families. It includes 9 heterogeneous reactions in the stratosphere/upper troposphere as in Carslaw et al. (1995). Monthly distributions of stratospheric sulphate aerosols followed the CMIP6 recommendations: concentration, surface area density, and volume density are based on the work of Thomason et al. (2018)

CMIP6 simulations have been run with a horizontal resolution in the atmosphere of about 1.4 degrees around the equator and 91 vertical levels with the highest level at 0.01 hPa and 39 levels above 100 hPa. Below 560 hPa halocarbon concentrations are relaxed towards prescribed global mean values. As a result, adjustment of halogen concentrations to reach the uniform atmospheric concentrations of 2014, as required by the piClim-HC protocol, took around 10 to 15 years.

3.2.3 GFDL-ESM4

The atmospheric component (AM4.1) of the GFDL Earth System Model version 4 (ESM4) is documented by Horowitz et al. (2020). The model has a horizontal resolution of approximately 100 km, using the GFDL Finite-Volume Cubed-Sphere dynamical core (Harris and Lin, 2013; Putman and Lin, 2007). The model has 49 hybrid sigma-pressure vertical levels, extending from the surface to 1 Pa. AM4.1 includes interactive tropospheric and stratospheric gas-phase and aerosol chemistry. The combined tropospheric and stratospheric chemistry scheme includes 18 prognostic (transported) bulk aerosol tracers, 58 prognostic gas-phase tracers, five prognostic ideal tracers, and 40 diagnostic (non-transported) chemical tracers, with 43 photolysis reactions, 190 gas-phase kinetic reactions, and 15 heterogeneous reactions. The tropospheric chemistry includes reactions of the NO_x–HO_x–O_x–CO–CH_4 system and oxidation schemes for other nonmethane volatile organic compounds. The stratospheric chemistry accounts for the major ozone loss cycles (O_x, HO_x, NO_x, ClO_x, and BrO_x). As described in Austin and Wilson (2010), heterogeneous reactions are included on ice and nitric acid trihydrate polar stratospheric clouds (PSCs) and in liquid ternary solution (LTS) aerosols. The PSCs are taken to be in thermodynamic equilibrium with the local conditions and calculated as in Hanson and Mauersberger (1988). The reaction rates in LTS are treated as in Carslaw et al. (1995). Mass accommodation coefficients and reaction probabilities are taken from Sander et al. (2006). Calculating the stratospheric

https://doi.org/10.5194/egusphere-2025-6033
Preprint. Discussion started: 15 January 2026

sources of reactive chlorine and bromine directly by transporting and photolyzing source gases (CFCs and halons) is computationally expensive and sensitive to any circulation biases in the model. Thus, for radiation calculations, global mean concentrations for ozone-depleting substances (ODSs, including CFC-11, CFC-12, CFC-113, and HCFC-22), as well as well-mixed greenhouse gases (GHGs), are specified from Meinshausen et al. (2017). Global mean concentrations of N_2O and CH_4 are specified at the surface level, with the atmospheric distributions simulated accounting for photochemical losses and transport. Simulated concentrations of N_2O and CH_4 are used for radiation calculations. The source of reactive chlorine and bromine species seen by the chemistry is parameterized as a function of tropospheric concentrations of source gases (lagged by the stratospheric "age of air"), as described in Appendix A of Austin and Wilson (2010). The parameterization uses observed source gas distributions to estimate, essentially, the fractional rate at which source gases entering the stratosphere are photolyzed and converted into reactive halogen species along their transport path through the stratosphere. The halogen source gases accounted for include CFC-11, CFC-12, CFC-113, CCl_4, CH_3Cl, CH_3CCl_3. HCFC-22, and lumped species accounting for additional Cl-containing (CFC-114, CFC-115, HCFC-141b + HCFC-142b) and Br-containing (Halon-1211, Halon-1301, Halon-2402, CH_3Br) species.

3.2.4 UKESM1-0-LL

The UKESM1 model (Sellar et al., 2019) uses the UK Chemistry and Aerosol (UKCA) stratosphere-troposphere gas-phase chemistry scheme called StratTropv1.0 (Archibald et al., 2020). For chemistry, UKESM1-0-LL lumps chlorinated species into CFC-11 and CFC-12 and brominated species into CH_3Br (Table 2 of Archibald et al., 2020). The surface concentrations of these are specified as lower boundary conditions. The stratospheric chemistry is described in detail in Morgenstern et al. (2009) with 85 hybrid height levels from the surface up to the model lid at 85 km. However, near-global total column ozone was biased high relative to other CMIP6 models throughout the historical period (Keeble et al., 2021) and the stratospheric ozone response to increasing concentrations of ODSs was strongly negative (Morgenstern et al., 2020), resulting in UKESM1-0-LL having a negative present-day ozone forcing (Skeie et al., 2020), i.e. the negative forcing from stratospheric ozone reduction outweighs the positive forcing from increases in tropospheric ozone.

For radiation calculations, global mean concentrations from Meinshausen et al. (2017) for ozone-depleting substances were lumped into CFC12 and HFC134a (Archibald et al., 2020) and prescribed alongside CO_2. Global mean concentrations of N_2O and CH_4 are specified at the surface. Transport and photochemical loss processes control their atmospheric concentrations which are also used in the radiation calculations. Ozone concentrations are calculated online from the simulated chemistry and used in radiation calculations.

3.2.5 GISS E2-1-G

https://doi.org/10.5194/egusphere-2025-6033
Preprint. Discussion started: 15 January 2026

The version of the model used here is documented in (Kelley et al., 2020), which describes updates to the chemistry since the fuller description found in Shindell et al. (2013b). Simulations were run with an atmospheric resolution of 2º latitude × 2.5º longitude, and 40 vertical layers gradually transitioning from terrain-following to constant pressure levels. Nominally, 17 layers are stratospheric, with a model top at 0.1 hPa. This model configuration transports 60+ prognostic gas and aerosol tracers, simulating tropospheric and stratospheric chemistry of 50+ gas-phase chemical species via 150+ reactions, including 28 photolysis reactions (based on the Fast-J2 scheme of Bian and Prather (2002) selectively updated through version Fast-JX 6.8d.) The GISS chemistry scheme uses reactive families for computational efficiency (ClOx, BrOx, HOx, NOx), only transporting the total family concentration, and explicitly represents 8 chlorinated species and 4 brominated species. The model includes heterogeneous reactions on both sulphate aerosols and PSCs. Surface areas available for reactions on PSCs are parameterized as a function of water vapour, temperature and HNO_3 (Hanson and Mauersberger, 1988).

The model's chemistry experiences changes in ODS through prescribed variation of CFC-11 and CFC-12 model input, consistent with that used by the radiation code, applied in the chemistry as a lower boundary condition. The sum of these species is scaled upward to represent implicitly included species by a factor of ~2.17 (=1722 ppt/794 ppt) and then used as a proxy for total available ODS halocarbons. For example, the anthropogenic halocarbons would be zero in preindustrial, but in 2014 would be: 2.17 × (0.233 ppb CFC-11 + 0.521 ppb CFC-12) or 1.63 ppb total available halocarbon chlorine. The model assigns a total Cl yield of 3.0 ppb per 1.8 ppb halocarbon photolyzed, with an additional 0.8 ppb from natural CH_3Cl. For bromine, the chemistry assigns a total Br yield of 4.5 ppt per 1.8 ppb halocarbon photolyzed (plus 0.5 ppt from natural CH_3Br). All these sources depend vertically on photolysis. In other words, the total available Cl or Br at a given altitude is determined by the fraction of CFC-11+CFC-12 that has been removed at that altitude relative to the surface where the CFC concentrations were prescribed.

As described above, the ODS are driven by prescribing the surface values of CFC. However, that chemical species is initialized consistent with radiation code's GHGs throughout the atmosphere, which would have contributed to the observed faster ozone equilibration compared to other models in this study, potentially aided by a fast circulation at this model resolution (Orbe et al., 2020).

3.2.6 MRI-ESM2

The atmospheric component of MRI ESM2-0 consists of three major component models: an atmospheric general circulation model with land processes (MRI-AGCM3.5), an aerosol chemical transport model (MASINGAR mk-2r4c) and an atmospheric chemistry model (MRI-CCM2.1) (Yukimoto et al., 2019). MRI-ESM2-0 uses different horizontal resolutions in each atmospheric component model but employs the same vertical resolution: MRI-AGCM3.5, MASINGAR mk-2r4c, and MRI-CCM2.1 use Tl159 (approximately 1.125◦ × 1.125◦), Tl95 (approximately 1.875◦ × 1.875◦) and T42 (approximately 2.8125◦ × 2.8125◦), respectively, and all models employ 80 vertical layers, with a model top at 0.01 hPa. The atmospheric chemistry

https://doi.org/10.5194/egusphere-2025-6033
Preprint. Discussion started: 15 January 2026

model, MRI- CCM2.1, calculates the evolution and distribution of the ozone and other trace gases in the troposphere and middle atmosphere (Deushi and Shibata, 2011; Yukimoto et al., 2019). The model includes 64 prognostic chemical species and 24 diagnostic chemical species, with 184 gas-phase reactions, 59 photolysis reactions and 16 heterogeneous reactions. It explicitly treats 4 chlorinated species (CFC-11, CFC-12, CCl4 and CH3Cl) and 3 brominated species (CH3Br, H1211 and H1301). The concentrations of these are scaled up to represent the total chlorine and bromine of 14 chlorinated and 4 brominated species, and are specified as a lower boundary condition in the model.

4 Results

4.1 Ozone changes

The changes in annual mean ozone between the last 30 years of the *piClim-control* and *piClim-HC* experiments are shown in Figure 2. The figure shows the expected latitude-height impact of halogens on ozone. Ozone depletion can be seen in the mid-upper stratosphere at all latitudes (due to gas-phase ClO + O chemistry) and in the lower stratosphere at higher latitudes (poleward of around 60°, related to winter/spring PSC processing). There are, however, considerable differences in the overall magnitude of the model responses with a global annual mean total column change of -14 DU in MRI-ESM-0 and -40 DU in UKESM1-0-LL (Thornhill et al., 2021b). There are also differences in the proportion of the response occurring in the lower stratosphere vs mid-upper stratosphere, with UKESM1-0-LL showing particularly strong Antarctic ozone depletion (Keeble et al., 2021).

https://doi.org/10.5194/egusphere-2025-6033
Preprint. Discussion started: 15 January 2026

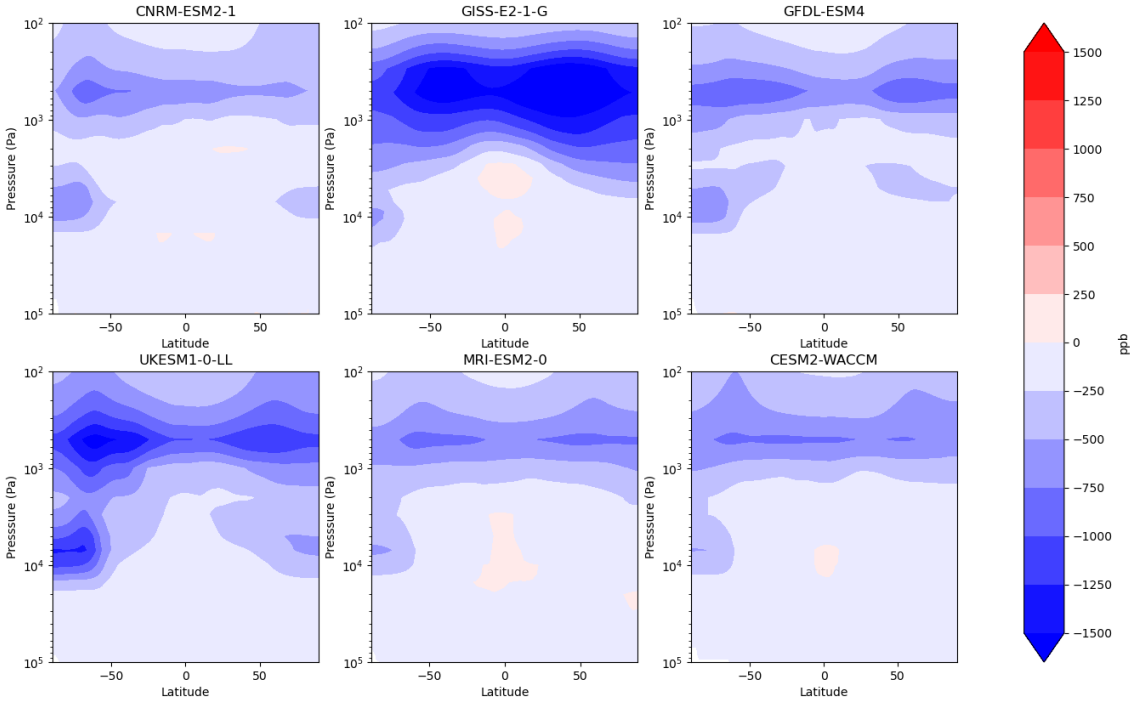

Figure 2: Change in ozone in ppb between the piClim-control and the piClim-HC experiments. Annual means averaged over the last 30 years of the simulations.

4.2 Ozone radiative forcing

As discussed in Section 1, the ozone radiative forcing from the *piClim-HC* experiments was documented in Thornhill et al. (2021b) and was based on the offline quantification of SARF using radiative kernels from Skeie et al. (2020). However, Collins et al. (2025) found that for ozone responses to changes in halocarbons, the ERF as diagnosed in ESMs was approximately twice the offline SARF. While an ozone-only ERF was not available from the Thornhill et al. (2021b) study, the total ERF was available. As well as the ozone ERF, this total ERF will include the direct contribution from halocarbons and also from any changes in aerosols. These ERFs are shown as function of the ozone offline SARF in Figure 3. The ERF and offline SARF are strongly correlated with a least-squares fit slope of 2.0 ± 0.4, supporting the factor of two difference between ERF and offline SARF. The intercept is 0.41 ± 0.07 Wm^{-2}, in agreement with Morgenstern et al. (2021) who attributed this to the direct ERF from halocarbons. As in the Morgenstern et al. (2021) study, the CNRM-ESM2-1 ERF is more negative than would be expected from the offline SARF or from the change in ozone column. The UKESM1-0-LL model has the strongest ozone

https://doi.org/10.5194/egusphere-2025-6033
Preprint. Discussion started: 15 January 2026

depletion and hence a negative total ERF due to halocarbon changes, but it still lies on the 2:1 line suggesting the relationship between ERF and offline SARF holds even for levels of ozone depletion that are larger than observed.

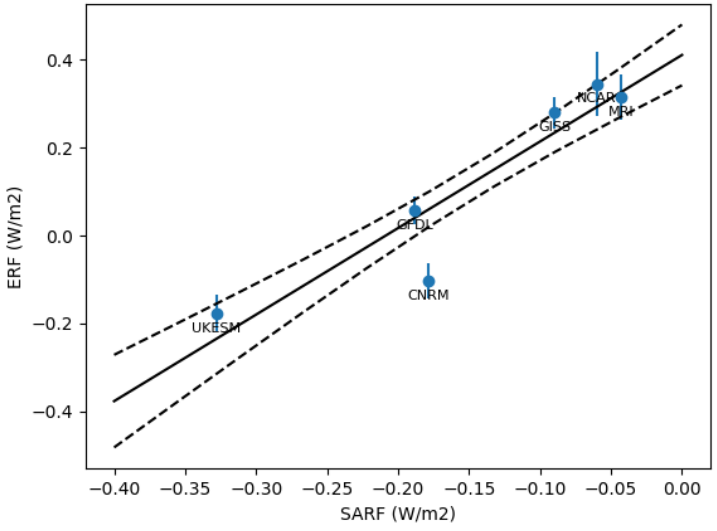

Figure 3: ERF vs ozone offline SARF for the *piClim-HC* minus *piClim* experiments for the six models. Values and uncertainties from (Thornhill et al., 2021b)**. Uncertainties are standard deviations of the annual mean ERF values. Uncertainties in the offline SARF are negligible. The solid line is a least-squares linear fit. The dashed lines are the 1 s.d. uncertainties.**

The large inter-model spread in the ERFs and offline SARFs reflects the variability in the modelled ozone depletion. Morgenstern et al. (2021) were able to use the model's simulated historical ozone depletion to derive an empirically constrained total ERF of 0.084 ± 0.059 Wm^{-2}. By subtracting their assessment of the direct halocarbon ERF (0.41 ± 0.07 Wm^{-2}) this gives an ozone ERF of -0.326 ± 0.09 Wm^{-2}.

The 1850 to 2014 changes in halocarbon concentrations are implemented in the models in different ways, with some models using fairly explicit schemes (such as CESM2-WACCM) where the concentrations of individual ODSs follow Meinshausen et al. (2017), and some (such as UKESM1-0-LL and GISS-E2-1) applying scaled changes to CFC-11 and CFC-12 to represent species that are not modelled. The species concentration changes applied in each model are listed in Table S1. These are converted to rates of emission of equivalent chlorine using: $(n_{\mathrm{Cl}} + \alpha n_{\mathrm{Br}}) \times \Delta C \times \frac{1}{\tau} \times \frac{m_{\mathrm{Cl}}}{m_{\mathrm{air}}} \times M_{\mathrm{atm}} \times \frac{\bar{C}}{C}$ as in Equation 3 (α is taken to be 60 (WMO 2022)), and are listed in Table S2. The fill factor $\left(\frac{\bar{C}}{C}\right)$ is estimated as a function of τ_{strat} based on an empirical fit (Eqn S3) to values in Volk et al. (1997) as described in the section S2. The fill factor is not applied for models using a constant height profile for halocarbons (GFDL-ESM4, MRI_ESM2). Following the IOD formulation, the ratio $\left(\frac{\tau}{\tau_{\mathrm{strat}}}\right)$ is used to convert these emissions into a stratospheric source of Cl which can be summed across all species to generate a total

https://doi.org/10.5194/egusphere-2025-6033
Preprint. Discussion started: 15 January 2026

production of Cl in the stratosphere (Table S3). This stratospheric Cl production is shown in Table S4 along with changes in the ozone column and offline SARF from Thornhill et al. (2021b). Although the concentrations in all models are ultimately derived from the Meinshausen et al. (2017) dataset, the different implementation in the models leads to different levels of Cl production in the stratosphere. The multi-model mean and standard deviation is 0.33 ± 0.03 Tg(Cl) yr^{-1}.

The total ozone column change allows us to calculate the efficiency of chlorine to deplete ozone (constant K in the IOD formula). This varies by a factor of 3 from 38 DU yr $Tg(Cl)^{-1}$ (MRI-ESM2) to 120 DU yr $Tg(Cl)^{-1}$ (UKESM1-0-LL). The wide variation in efficiency to deplete ozone when normalised by the chlorine change implies that the differences in ozone concentrations in Figure 2 are due to differences in the model chemical mechanisms rather than differences in chlorine sources. The value of 120 DU yr $Tg(Cl)^{-1}$ for the UKESM1-0-LL model is similar to the K of 100 ± 16 DU yr $Tg(Cl)^{-1}$ found in Pyle et al. (2022) which used a version of the same model. The strong response of the UKESM1-0-LL model was reported in Keeble et al. (2021).

The multi-model mean offline SARF in Table S4 is -0.15 ± 0.10 Wm^{-2} (as in Thornhill et al. (2021b)) where the uncertainty reflects the inter-model standard deviation. This is less than half the empirically constrained ERF from Morgenstern et al. (2021), with comparable absolute uncertainty but much larger relative uncertainty. Combining the ERF with a mean total column change of -23.9 ± 8.9 DU gives a radiative efficiency (ERF) of 13.6 ± 6.3 mWm^{-2} DU^{-1}, in agreement with the radiative efficiency (ERF) due to stratospheric ozone recovery in Collins et al. (2025) of 16.4 ± 7.9 mWm^{-2} DU^{-1}.

The ERF divided by the stratospheric chlorine production gives the equilibrium ozone radiative forcing for a stratospheric chlorine source of 1 kg yr^{-1}, or equivalently the integrated radiative forcing for a pulse stratospheric source of 1 kg Cl. This has the characteristics of an $AGWP_\infty$ for a pulse production of chlorine atoms in the stratosphere (Table 1).

Table 1 Multi-model means of results from the piClim-HC minus piClim-control experiments: Cl production and total ozone column change (from Table S4), ozone ERF from Morgenstern et al. (2021), ozone effective radiative forcing efficiency per change in ozone column and ozone radiative efficiency per production of Cl.

	Cl production ($Tg(Cl)\ yr^{-1}$)	ΔO_3 (DU)	O_3 ERF (Wm^{-2})	ϕ_{O_3} ($mWm^{-2}\ DU^{-1}$)	$AGWP_\infty$ ($nWm^{-2}\ yr\ kg(Cl)^{-1}$)
Multi-model mean	0.32 ± 0.03	-23.9 ±8.9	-0.326 ± 0.09	13.6 ± 2.2	-1.01 ± 0.28

4.3 Methane lifetime change

Table 2 Multi-model (excluding CNRM-ESM2-1) means of results from the piClim-HC minus piClim-control experiments: Cl production and methane radiative forcing (from Table S5), methane radiative efficiency per production of Cl.

	Cl production ($Tg(Cl)\ yr^{-1}$)	CH_4 ERF (Wm^{-2})	$AGWP_\infty$ ($nWm^{-2}\ yr\ kg(Cl)^{-1}$)
Multi-model mean	0.32 ± 0.03	-0.066 ± 0.040	-0.21 ± 0.13

https://doi.org/10.5194/egusphere-2025-6033
Preprint. Discussion started: 15 January 2026

The effects of halocarbons on the fractional change in total methane lifetimes ($\Delta\tau_{CH4}/\tau_{CH4}$) are taken from Thornhill et al. (2021b) as are methane feedback factors f. These are shown in Table S5. The CNRM-ESM2-1 model does not account for methane oxidation in the lower troposphere and is excluded from these calculations. The model simulations used fixed methane concentrations, but implied changes in steady state concentrations ΔC can be calculated using $\Delta C \approx C \times f \frac{\Delta\tau}{\tau}$ (Thornhill et al., 2021a). These are converted to an ERF using a methane radiative efficiency of 0.00057 Wm^{-2} ppb^{-1} (which includes contributions to ozone and stratospheric water vapour) and a 2019 concentration of 1866 ppb (Forster et al., 2021).

There are wide variations in the effects on methane lifetime between models which do not seem strongly related to the change in ozone column. The CESM2-WACCM model has the largest methane lifetime change even though it has the second smallest change in ozone. This suggests that the variations in the tropospheric chemistry schemes play a significant role. Both methane lifetime change and ozone depletion act in the same sense, i.e. a decrease in radiative forcing.

Table 2 shows the multi-model mean methane ERF and (as was done for ozone), an $AGWP_{\infty}$ due to methane forcing for a pulse "emission" of chlorine atoms in the stratosphere. This is around a fifth of that due to ozone. The historical forcing of -0.066 ± 0.040 Wm^{-2} is slightly higher than the value of -0.051 Wm^{-2} in IPCC AR6 Table 6.SM.1 (Szopa et al. 2021) since they accounted for contributions of ozone and stratospheric water vapour responses to the methane lifetime effect separately whereas here we have combined them into a total methane lifetime effect.

Adding the ERFs from ozone and methane from Tables 1 and 2 gives a total indirect contributions of halocarbons to historical (to 2014) forcing of -0.39 ± 0.10 Wm^{-2}. This can be compared to the direct forcing (to 2019) of "gases covered by the Montreal Protocol" of 0.354 ± 0.067 Wm^{-2} in Forster et al., (2021), and would suggest that historically the Montreal Protocol gases have made a contribution to radiative forcing that is much smaller than their direct forcing would have indicated, with uncertainties in the net effect including negative and positive forcing values.

4.4 Saturation of polar depletion

Daniel et al. (1995), WMO (1994) and subsequent WMO Ozone Assessments assume that polar ozone depletion since 1990 has been saturated; so small perturbations in ODSs have no further effect on polar ozone depletion until polar EESC levels decline below 1990 levels. The date for this in WMO (2022) is 2038. For longer lived species such as CFC-12 this reduces the polar contribution to the indirect GWP100 by around 20% and hence the total (polar + extra-polar) contribution by around 10%. However, for shorter lived species such as methyl chloroform (lifetime of 5 years) the contribution to the polar EESC will have almost completely decayed by 2038. In the case of methyl chloroform the assumption of no additional polar ozone depletion until after 2038 would reduce the indirect ozone GWP100 by around 30%.

The ESMs used for the time slice *piClim-control* and *piClim-HC* experiments also conducted transient simulations of the historical period with all species evolving over this period *historical* and with all species except halocarbons evolving (which are fixed at 1950 levels) *hist-1950HC* (Collins et al., 2017). The differences in ozone between these two simulations do not

https://doi.org/10.5194/egusphere-2025-6033
Preprint. Discussion started: 15 January 2026

show a clear saturation of ozone depletion although the year-to-year variability is rather large, see Figure 4. The inclusion of a saturation effect for polar ozone depletion makes the GWP100 very sensitive to the assumed start year of the pulse. We therefore do not include this effect in the GWP calculations.

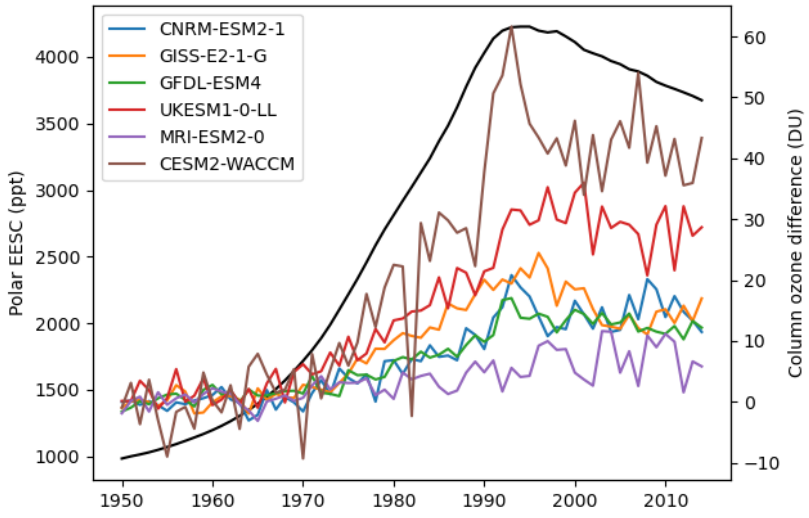

Figure 4. Polar (>60 °, north and south combined) total ozone column change (right hand axis) due to halocarbons (historical minus historical with halocarbons fixed at 1950 levels). Polar EESC is shown in black, offset by 10 years into the future (left hand axis). Polar EESC for this figure is calculated using ODS concentrations from (Meinshausen et al., 2017)**.**

5. Climate metrics

5.1 IOD-based

The total AGWP for a halocarbon is given by the sum of the direct AGWP and the indirect AGWPs from ozone depletion and methane lifetime changes. The chlorine $AGWP_\infty$ values from Tables 1 and 2 can be applied to the emission of any halocarbons since, using the IOD formulation in Equation 1, the amount of chlorine produced in the stratosphere for a pulse emission E of any gas is given by $(n_{\mathrm{Cl}} + \alpha n_{\mathrm{Br}}) \times \left(\frac{\tau}{\tau_{\mathrm{strat}}}\right) \times \frac{m_{\mathrm{Cl}}}{m} \times E$. The direct radiative efficiencies ϕ_{HC} for halocarbons are typically given per surface concentration and account for a decreased stratospheric concentration (Hodnebrog et al., 2020). For direct $AGWP_\infty$ (as we did for the OD_∞ calculation) we account for this as a slightly reduced emission needed to achieve the specified surface concentration. Therefore direct $AGWP_\infty$ for each halocarbon is calculated by $\phi_{HC} \times \frac{m_{\mathrm{air}}}{m} \times \frac{1}{M_{\mathrm{atm}} \times \frac{\bar{C}}{C}} \times \tau$, using Eqn S1 for $\frac{\bar{C}}{C}$.

https://doi.org/10.5194/egusphere-2025-6033
Preprint. Discussion started: 15 January 2026

Note accounting for a non-constant height profile is not typically done for AGWPs, e.g. (Forster et al., 2021), and will increase the AGWP of methane by about 3%, and that of CFC-11 by about 8% (Figure S1).

We assume a 3-year time delay for transport of halocarbons to the extra-polar stratosphere as in Daniel et al. (1995). There will be a further time lag for the photolysis of the halocarbons to lead to ozone destruction. Analysis of the three models that specify the surface concentrations of halocarbons shows that there is an approximately 3-year delay before ozone depletion starts, but that depletion takes further time to progress as the halocarbons are photolyzed in the stratosphere (Figure S2). The transport time simply delays the ozone depletion by 3-years, so the effective time horizon is reduced by 3 years, i.e the factor $\left(1-e^{-H/\tau}\right)$ becomes $\left(1-e^{-(H-\Delta t)/\tau}\right)$ where Δt is the time lag.

The GWP_{100} is then $AGWP_{\infty} \times \left(1-e^{-(100-\Delta t)/\tau}\right)/AGWP_{100}^{CO_2}$. The time lag is applied to the ozone depletion and methane lifetime effects, but not for the direct effect. Figure 5 shows the total GWP_{100} for five species (CFC-11, CFC-12, HCFC-22, CCl_4, Halon-1211) and the split into the direct effect of the halocarbon, the effect on ozone depletion and the effect on methane lifetime. These GWPs do not include carbon cycle feedbacks and so the direct contributions are not identical to the values in Forster et al. (2021) or WMO (2022). The same calculation for 304 different halocarbons is shown in Table S8. The indirect chemical effects are calculated using the multi-model mean sensitivities (Tables 1 and 2). For CFC-11 the best estimate GWP_{100} is negative when including the indirect effects although the one standard deviation uncertainty extends to zero. The indirect effects reduce the GWP_{100} for CFC-12 and HCFC-22 by about 38% and 28% respectively, with the net effect positive; for CCl_4 and Halon-1211 the indirect effects significantly outweigh the direct effects leading to negative GWP_{100}. We have not included the contribution from the radiatively active decay products of the halocarbons ($ClONO_2$, $COCl_2$, COF_2 and COClF), but from Thornhill et al. (2024) they could contribute +170, +190, +9 and +340 to the GWP_{100} for CFC-11, CFC-12, HCFC-22 and CCl_4 respectively.

For CFC-11 the high number of chlorine atoms and the shorter stratospheric lifetime mean that the cooling from ozone depletion is large enough to exceed, the direct effect. CFC-12 has approximately twice the stratospheric lifetime (103 years) of CFC-11 and 2 rather than 3 chlorine atoms, and HCFC-22 has a 120 years stratospheric lifetime and only 1 chlorine atom so both have stronger warming than cooling. CCl_4 has only a 44 year stratospheric lifetime and 4 chlorine atoms, and Halon-1211 contains a bromine atom which has 60 times the ozone depleting potential as chlorine and so are both strongly cooling. From the total GWPs in Table S8, most CFCs are warming (high radiative efficiencies and long stratospheric lifetimes). Many HCFCs cause a net cooling due to lower radiative efficiencies and shorter stratospheric lifetimes. Chlorocarbons and hydrochlorocarbons are cooling; chlorine-containing halogenated ethers are warming; all brominated species are cooling.

https://doi.org/10.5194/egusphere-2025-6033
Preprint. Discussion started: 15 January 2026

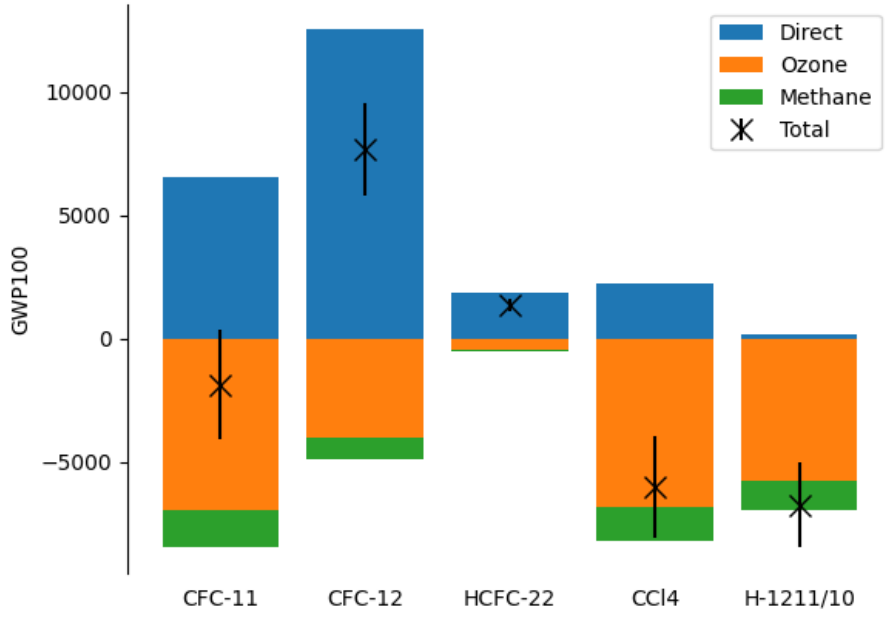

Figure 5. GWP100 direct and indirect contributions for 5 illustrative halocarbons based on IOD calculations, using values from Table S8. Values for Halon-1211 are divided by 10 to keep them on the same scale.

5.2 EESC-based

Here we repeat the GWP calculations using EESC. As in Daniel et al. (1995) we assume that 40% of the radiative forcing is due to polar ozone depletion and 60% to extra-polar depletion. Table S4 shows the 1850 to 2014 changes in polar and extra-polar EESC values for each model. EESC values use Equation 7 with fractional release values from Engel et al. (2018). The EESC values are based on the specified fixed concentrations used in the model setup. This is not exactly the same methodology as in Engel et al. (2018) which is based on evolving concentrations. This may be an issue for models that specify the concentrations in the stratosphere rather than transporting concentrations from the surface. However we maintain this formulation for consistency with WMO (2022). We calculate separate radiative efficiencies for polar $\phi_{O_3}^{\text{polar}}$ and extra-polar $\phi_{O_3}^{\text{extra-polar}}$ ozone depletion, and for methane destruction ϕ_{CH_4} (using extra-polar EESC concentrations) in Wm^{-2} ppt(Cl) – see Table S5. The components of the indirect AGWP_{∞} are then given by

https://doi.org/10.5194/egusphere-2025-6033
Preprint. Discussion started: 15 January 2026

$AGWP_{\infty}^{i}=(n_{Cl}+\alpha n_{Br})\times f\times\tau\times\frac{m_{air}}{m}\times\frac{1}{M_{atm}\times\frac{C}{C}}\times\phi^{i}$, where the *i* components are polar ozone, extra-polar ozone and methane.

As for IOD, the GWP_{100} is $AGWP_{\infty}\times\left(1-e^{(100-\Delta t)/\tau}\right)/AGWP_{100}^{CO_2}$ with a 3 year time lag for extra-polar ozone and methane. For polar ozone a 5.5 year time lag accounts for the extra time for transport to the poles.

The EESC and IOD approaches give different relative weighting to the different halocarbons. The indirect GWP_{100} values are similar to those calculated using IOD, confirming the near proportionality of extra-polar f and $\frac{1}{\tau_{strat}}$ found in Section 2. There is an increased (negative) contribution from ozone to the CFC-11 and CFC-12 values coming from the polar depletion. This is because the polar f is relatively large even though the stratospheric lifetime is long. There is also a decreased contribution from ozone and methane to the HCFC-22 GWP since the extra-polar f is lower than expected from the stratospheric lifetime (see Fig. 1). Neither of these differences are significant compared to the large uncertainties in the modelled ozone and methane responses.

Table 3 GWP100 indirect contributions based on EESC calculations for 5 illustrative halocarbons. The ozone contribution is split into polar and extra-polar values. The direct contributions are the same as in Table S8.

Species	Direct	O_3-extra-polar	O_3-polar	O_3	CH_4	Total
CFC-11	6565 ± 756	-4749 ± 1311	-2688 ± 742	-7437 ± 2053	-1706 ± 1087	-2577 ± 2443
CFC-12	12510 ± 1441	-2553 ± 705	-2470 ± 682	-5023 ± 1387	-917 ± 584	6571 ± 2083
HCFC-22	1890 ± 218	-205 ± 57	-163 ± 45	-369 ± 102	-74 ± 47	1448 ± 245
CCl_4	2213 ± 255	-4450 ± 1228	-2147 ± 593	-6596 ± 1821	-1598 ± 1019	-5981 ± 2102
Halon-1211	2052 ± 236	-40664 ± 11226	-18345 ± 5065	-59009 ± 16291	-14605 ± 9309	-71562 ± 18764

6. Discussion and conclusions

Calculations of the indirect GWPs of ODSs have typically mixed observed changes in EESC with model calculations of the stratospheric ozone forcing (Daniel et al., 1995). Here we have used a pure modelling approach (based on the CMIP6 *piClim-HC* experiment) to be consistent and have explicitly separated the terms due to the radiative forcing of the ozone changes and those due to the decreases in methane lifetime.

We use the effective radiative forcing (ERF) calculated online in the models rather than the more usual offline-calculated stratospheric-temperature adjusted radiative forcing (SARF) as Collins et al. (2025) find that for ozone responses to halocarbons the offline SARF underestimates the ERF by a factor of two, and we find a similar factor when correlating ERF and offline SARF from the *piCim-HC* experiment. Collins et al. (2025) were not able to conclusively explain the cause of the difference between ERF and offline SARF, but noted that since the ERF was closer to the instantaneous forcing (IRF) the fixed

https://doi.org/10.5194/egusphere-2025-6033
Preprint. Discussion started: 15 January 2026

dynamical heating (FDH) calculation used in the offline SARF might be overestimating the stratospheric temperature adjustment and hence underestimating the net forcing. The one ESM that diagnosed this found a much weaker stratospheric temperature response over the Antarctic than that generated by FDH, but a stronger response in the tropics. Individual adjustment terms for the *piClim-HC* experiment were reported in Thornhill et al. (2021b) and show that the ERF and online-calculated SARF (subtracting all adjustments except stratospheric temperature from the ERF) were similar. This suggests that for changes in stratospheric ozone the main difference is not between the ERF and the SARF, but between the online and offline calculations of SARF. Additional future research to further understand the underlying causes of this difference would be valuable.

There is a very wide range of model responses for both the ozone radiative forcing and in the methane lifetime change. We have used the emergent constraint of Morgenstern et al. (2021) to reduce the uncertainty on the ozone ERF, but use the multi-model standard deviation to estimate the uncertainty in the methane ERF. This leads to a net indirect ERF from historical increases in Montreal Protocol gases that completely offsets the positive direct ERF. This finding differs from that in Western et al. (in review) who found a positive total forcing from halocarbons when using the less negative offline SARF to estimate the ozone contribution. Since the direct and indirect ERFs from halocarbons and ozone depletion have very different spatial structures a near zero net ERF can still imply regional temperature impacts. This near zero ERF from Montreal Protocol gases also does not mean that the Montreal Protocol itself has had no climate impact. In a scenario without the Montreal Protocol "World avoided" Velders et al. (2007) comment that at much higher levels of halocarbon concentrations the ozone depletion patterns are likely to be different to those currently observed. In that case the linear framework used in this paper would not be valid.

Note that using the Morgenstern et al. (2021) ERF rather than the Skeie et al. (2020) offline SARF to quantify the contribution of stratospheric ozone depletion would reduce the historical ozone forcing from 0.47 ± 0.23 Wm^{-2} in Forster et al. (2021) to 0.29 ± 0.27 Wm^{-2} (90% confidence level).

The IOD (Pyle et al., 2022) uses model-derived quantities (atmospheric and stratospheric lifetimes) to determine the integrated ozone depletion for a pulse emission and so can be applied to generate indirect GWPs for any halocarbon for which these lifetimes have been quantified. Table A5 of WMO (2022) lists these for 304 ozone-depleting species and the GWP100 values for each of these are shown in Table S8. We find that indirect GWPs are approximately twice as large as those assessed in WMO (2022) due mainly to the use of ozone ERF rather than offline SARF. This means that the net GWP100 for CFC-11 is negative, and that for CFC-12 is positive, but reduced (by around 15%) compared to WMO (2022). Species with lower direct radiative efficiencies and shorter stratospheric lifetimes will have negative GWPs.

GWP100 values have also been calculated using the EESC formulation (Daniel et al., 1995) which requires the use of fractional release factors that are generally observationally based; these values might differ from those implicit in the models and thus the results might differ from the IOD results, which can be calculated purely from models. The assumptions in the EESC

https://doi.org/10.5194/egusphere-2025-6033
Preprint. Discussion started: 15 January 2026

formulation might not be applicable to models specifying the stratospheric concentrations of halocarbons. However the indirect GWP100 values are consistent within the uncertainties between the IOD and EESC formulations.

The IOD metric as currently formulated cannot distinguish between polar and extra-polar ozone depletion. The assumption that halocarbon perturbations have no additional impacts on polar ozone depletion until 2038 in WMO (2022) has significant effects on the indirect GWP100 for short-lived species, i.e. those for which a pulse emission will have mostly decayed away by 2038. As the ESMs do not show conclusive evidence for such a saturation effect, perhaps because of large interannual variability, it is unclear whether the inability to distinguish between polar and extra-polar depletion in the IOD metric is of much concern.

Data Availability

The model data from Phase 6 of the Coupled Model Intercomparison Project (CMIP6) used in this study are available through the Earth System Grid Federation

Acknowledgements

WJC, MPC, JW and ZW were supported by the UK Natural Environment Research Council (NERC) Grant "Investigating Halocarbon Impacts on the global environment" (Grant Reference NE/X004198/1 for WJC and JW, NE/X003450/1 for MPC and ZW). FMO'C was supported by the European Union's Horizon 2020 project ESM2025 (under grant agreement No 101003536) and the Met Office Hadley Centre Climate Programme funded by DSIT, UK. ØH was supported by the Research Council of Norway (project no. 336227). Climate modelling at GISS is supported by the NASA Modeling, Analysis and Prediction program. GISS simulations used resources provided by the NASA High-End Computing (HEC) Program through the NASA Center for Climate Simulation (NCCS) at Goddard Space Flight Center.

Author contributions

WJC designed the study with consultation and input from JSD. The IOD formulation was devised by MPC and ZW. The original CMIP6 model simulations were conducted by MC, MD, GF, PG, LWH, JK, DK, VN, FMO'C, DS, ST, and KT. Data analysis and construction of figures was by WJC. All authors were involved in drafting and reviewing the manuscript.

Competing interests

Some authors are members of the editorial board of Atmospheric Chemistry and Physics.

https://doi.org/10.5194/egusphere-2025-6033
Preprint. Discussion started: 15 January 2026

References

Archibald, A. T., O'Connor, F. M., Abraham, N. L., Archer-Nicholls, S., Chipperfield, M. P., Dalvi, M., Folberth, G. A., Dennison, F., Dhomse, S. S., Griffiths, P. T., Hardacre, C., Hewitt, A. J., Hill, R. S., Johnson, C. E., Keeble, J., Köhler, M. O., Morgenstern, O., Mulcahy, J. P., Ordóñez, C., Pope, R. J., Rumbold, S. T., Russo, M. R., Savage, N. H., Sellar, A., Stringer, M., Turnock, S. T., Wild, O., and Zeng, G.: Description and evaluation of the UKCA stratosphere–troposphere chemistry scheme (StratTrop vn 1.0) implemented in UKESM1, Geosci Model Dev, 13, 1223–1266, https://doi.org/10.5194/gmd-13-1223-2020, 2020.

Austin, J. and Wilson, R. J.: Sensitivity of polar ozone to sea surface temperatures and halogen amounts, Journal of Geophysical Research: Atmospheres, 115, 18303, https://doi.org/10.1029/2009JD013292, 2010.

Bian, H. and Prather, M. J.: Fast-J2: Accurate Simulation of Stratospheric Photolysis in Global Chemical Models, J Atmos Chem, 41, 281–296, https://doi.org/10.1023/A:1014980619462, 2002.

Carslaw, K. S., Luo, B., and Peter, T.: An analytic expression for the composition of aqueous HNO3-H2SO4 stratospheric aerosols including gas phase removal of HNO3, Geophys Res Lett, 22, 1877–1880, https://doi.org/10.1029/95GL01668, 1995.

Collins, W., Lamarque, J. F., Schulz, M., Boucher, O., Eyring, V., Hegglin, M., Maycock, A., Myhre, G., Prather, M., Shindell, D., and Smith, S.: AerChemMIP: Quantifying the effects of chemistry and aerosols in CMIP6, Geosci Model Dev, 10, 585–607, https://doi.org/10.5194/gmd-10-585-2017, 2017.

Collins, W. J., O'Connor, F. M., Byrom, R. E., Hodnebrog, Ø., Jöckel, P., Mertens, M., Myhre, G., Nützel, M., Olivié, D., Bieltvedt Skeie, R., Stecher, L., Horowitz, L. W., Naik, V., Faluvegi, G., Im, U., Murray, L. T., Shindell, D., Tsigaridis, K., Abraham, N. L., and Keeble, J.: Climate forcing due to future ozone changes: an intercomparison of metrics and methods, Atmos Chem Phys, 25, 9031–9060, https://doi.org/10.5194/acp-25-9031-2025, 2025.

Danabasoglu, G., Lamarque, J. F., Bacmeister, J., Bailey, D. A., DuVivier, A. K., Edwards, J., Emmons, L. K., Fasullo, J., Garcia, R., Gettelman, A., Hannay, C., Holland, M. M., Large, W. G., Lauritzen, P. H., Lawrence, D. M., Lenaerts, J. T. M., Lindsay, K., Lipscomb, W. H., Mills, M. J., Neale, R., Oleson, K. W., Otto-Bliesner, B., Phillips, A. S., Sacks, W., Tilmes, S., van Kampenhout, L., Vertenstein, M., Bertini, A., Dennis, J., Deser, C., Fischer, C., Fox-Kemper, B., Kay, J. E., Kinnison, D., Kushner, P. J., Larson, V. E., Long, M. C., Mickelson, S., Moore, J. K., Nienhouse, E., Polvani, L., Rasch, P. J., and Strand, W. G.: The Community Earth System Model Version 2 (CESM2), J Adv Model Earth Syst, 12, https://doi.org/10.1029/2019MS001916, 2020.

Daniel, J. S., Solomon, S., and Albritton, D. L.: On the evaluation of halocarbon radiative forcing and global warming potentials, J Geophys Res, 100, https://doi.org/10.1029/94JD02516, 1995.

Deushi, M. and Shibata, K.: Impacts of increases in greenhouse gases and ozone recovery on lower stratospheric circulation and the age of air: Chemistry-climate model simulations up to 2100, Journal of Geophysical Research Atmospheres, 116, https://doi.org/10.1029/2010JD015024, 2011.

https://doi.org/10.5194/egusphere-2025-6033
Preprint. Discussion started: 15 January 2026

Emmons, L. K., Schwantes, R. H., Orlando, J. J., Tyndall, G., Kinnison, D., Lamarque, J. F., Marsh, D., Mills, M. J., Tilmes, S., Bardeen, C., Buchholz, R. R., Conley, A., Gettelman, A., Garcia, R., Simpson, I., Blake, D. R., Meinardi, S., and Pétron, G.: The Chemistry Mechanism in the Community Earth System Model Version 2 (CESM2), J Adv Model Earth Syst, https://doi.org/10.1029/2019MS001882, 2020.

Engel, A., Bönisch, H., Ostermöller, J., Chipperfield, M. P., Dhomse, S., and Jöckel, P.: A refined method for calculating equivalent effective stratospheric chlorine, Atmos Chem Phys, 18, 601–619, https://doi.org/10.5194/acp-18-601-2018, 2018.

Eyring, V., Bony, S., Meehl, G. A., Senior, C. A., Stevens, B., Stouffer, R. J., and Taylor, K. E.: Overview of the Coupled Model Intercomparison Project Phase 6 (CMIP6) experimental design and organization, Geosci Model Dev, https://doi.org/10.5194/gmd-9-1937-2016, 2016.

Fels, S. B., Mahlman, J. D., Schwarzkopf, M. D., and Sinclair, R. W.: Stratospheric Sensitivity to Perturbations in Ozone and Carbon Dioxide: Radiative and Dynamical Response, J Atmos Sci, 37, 2265–2297, https://doi.org/10.1175/1520-0469(1980)037<2265:SSTPIO>2.0.CO;2, 1980.

Forster, P., Ramaswamy, V., Artaxo, P., Berntsen, T., Betts, R., Fahey, D. W., Haywood, J., Lean, J., Lowe, D. C., and Myhre, G.: Chapter 2. Changes in atmospheric constituents and in radiative forcing, Climate Change 2007. The Physical Science Basis, 20, 2007.

Forster, P., Storelvmo, T., Armour, K., Collins, W., Dufresne, J.-L., Frame, D., Lunt, D. J., Mauritsen, T., Palmer, M. D., Watanabe, M., Wild, M., and Zhang, H.: The Earth's Energy Budget, Climate Feedbacks and Climate Sensitivity, in: Climate Change 2021: The Physical Science Basis. Contribution of Working Group I to the Sixth Assessment Report of the Intergovernmental Panel on Climate Change, edited by: Masson-Delmotte, V., Zhai, P., Pirani, A., Connors, S. L., Pean, C., Berger, S., Caud, N., Chen, Y., Goldfarb, L., Gomis, M. I., Huang, M., Leitzell, K., Lonnoy, E., Matthews, J. B. R., Maycock, T. K., Waterfield, T., Yelekci, O., Yu, R., and Zhou, B., Cambridge University Press, Cambridge, United Kingdom and New York, NY, USA, 923–1054, 2021.

Gettelman, A., Mills, M. J., Kinnison, D. E., Garcia, R. R., Smith, A. K., Marsh, D. R., Tilmes, S., Vitt, F., Bardeen, C. G., McInerney, J., Liu, H. -L., Solomon, S. C., Polvani, L. M., Emmons, L. K., Lamarque, J. -F., Richter, J. H., Glanville, A. S., Bacmeister, J. T., Phillips, A. S., Neale, R. B., Simpson, I. R., DuVivier, A. K., Hodzic, A., and Randel, W. J.: The Whole Atmosphere Community Climate Model Version 6 (WACCM6), Journal of Geophysical Research: Atmospheres, https://doi.org/10.1029/2019jd030943, 2019.

Hanson, D. and Mauersberger, K.: Laboratory studies of the nitric acid trihydrate: Implications for the south polar stratosphere, Geophys Res Lett, 15, 855–858, https://doi.org/10.1029/GL015I008P00855, 1988.

Harris, L. M. and Lin, S. J.: A Two-Way Nested Global-Regional Dynamical Core on the Cubed-Sphere Grid, Mon Weather Rev, 141, 283–306, https://doi.org/10.1175/MWR-D-11-00201.1, 2013.

https://doi.org/10.5194/egusphere-2025-6033
Preprint. Discussion started: 15 January 2026

Hodnebrog, Aamaas, B., Fuglestvedt, J. S., Marston, G., Myhre, G., Nielsen, C. J., Sandstad, M., Shine, K. P., and Wallington, T. J.: Updated Global Warming Potentials and Radiative Efficiencies of Halocarbons and Other Weak Atmospheric Absorbers, Reviews of Geophysics, 58, e2019RG000691, https://doi.org/10.1029/2019RG000691, 2020.

Horowitz, L. W., Naik, V., Paulot, F., Ginoux, P. A., Dunne, J. P., Mao, J., Schnell, J., Chen, X., He, J., John, J. G., Lin, M., Lin, P., Malyshev, S., Paynter, D., Shevliakova, E., and Zhao, M.: The GFDL Global Atmospheric Chemistry-Climate Model AM4.1: Model Description and Simulation Characteristics, J Adv Model Earth Syst, 12, e2019MS002032, https://doi.org/10.1029/2019MS002032, 2020.

Keeble, J., Hassler, B., Banerjee, A., Checa-Garcia, R., Chiodo, G., Davis, S., Eyring, V., Griffiths, P. T., Morgenstern, O., Nowack, P., Zeng, G., Zhang, J., Bodeker, G., Burrows, S., Cameron-Smith, P., Cugnet, D., Danek, C., Deushi, M., Horowitz, L. W., Kubin, A., Li, L., Lohmann, G., Michou, M., Mills, M. J., Nabat, P., Olivié, D., Park, S., Seland, Ø., Stoll, J., Wieners, K. H., and Wu, T.: Evaluating stratospheric ozone and water vapour changes in CMIP6 models from 1850 to 2100, Atmos Chem Phys, 21, 5015–5061, https://doi.org/10.5194/ACP-21-5015-2021, 2021.

Kelley, M., Schmidt, G. A., Nazarenko, L. S., Bauer, S. E., Ruedy, R., Russell, G. L., Ackerman, A. S., Aleinov, I., Bauer, M., Bleck, R., Canuto, V., Cesana, G., Cheng, Y., Clune, T. L., Cook, B. I., Cruz, C. A., Del Genio, A. D., Elsaesser, G. S., Faluvegi, G., Kiang, N. Y., Kim, D., Lacis, A. A., Leboissetier, A., LeGrande, A. N., Lo, K. K., Marshall, J., Matthews, E. E., McDermid, S., Mezuman, K., Miller, R. L., Murray, L. T., Oinas, V., Orbe, C., García-Pando, C. P., Perlwitz, J. P., Puma, M. J., Rind, D., Romanou, A., Shindell, D. T., Sun, S., Tausnev, N., Tsigaridis, K., Tselioudis, G., Weng, E., Wu, J., and Yao, M. S.: GISS-E2.1: Configurations and Climatology, J Adv Model Earth Syst, 12, https://doi.org/10.1029/2019MS002025, 2020.

Kinnison, D. E., Brasseur, G. P., Walters, S., Garcia, R. R., Marsh, D. R., Sassi, F., Harvey, V. L., Randall, C. E., Emmons, L., Lamarque, J. F., Hess, P., Orlando, J. J., Tie, X. X., Randel, W., Pan, L. L., Gettelman, A., Granier, C., Diehl, T., Niemeier, U., and Simmons, A. J.: Sensitivity of chemical tracers to meteorological parameters in the MOZART-3 chemical transport model, Journal of Geophysical Research Atmospheres, 112, https://doi.org/10.1029/2006JD007879, 2007.

Meinshausen, M., Vogel, E., Nauels, A., Lorbacher, K., Meinshausen, N., Etheridge, D. M., Fraser, P. J., Montzka, S. A., Rayner, P. J., Trudinger, C. M., Krummel, P. B., Beyerle, U., Canadell, J. G., Daniel, J. S., Enting, I. G., Law, R. M., Lunder, C. R., O'Doherty, S., Prinn, R. G., Reimann, S., Rubino, M., Velders, G. J. M., Vollmer, M. K., Wang, R. H. J., and Weiss, R.: Historical greenhouse gas concentrations for climate modelling (CMIP6), Geosci Model Dev, 10, https://doi.org/10.5194/gmd-10-2057-2017, 2017.

Michou, M., Saint-Martin, D., Teyssèdre, H., Alias, A., Karcher, F., Olivié, D., Voldoire, A., Josse, B., Peuch, V.-H., Clark, H., Lee, J. N., and Chéroux, F.: A new version of the CNRM Chemistry-Climate Model, CNRM-CCM: description and improvements from the CCMVal-2 simulations, Geosci Model Dev, 4, 873–900, https://doi.org/10.5194/gmd-4-873-2011, 2011.

https://doi.org/10.5194/egusphere-2025-6033
Preprint. Discussion started: 15 January 2026

Michou, M., Nabat, P., Saint-Martin, D., Bock, J., Decharme, B., Mallet, M., Roehrig, R., Séférian, R., Sénési, S., and Voldoire, A.: Present-Day and Historical Aerosol and Ozone Characteristics in CNRM CMIP6 Simulations, J Adv Model Earth Syst, 12, e2019MS001816, https://doi.org/10.1029/2019MS001816, 2020.

Mills, M. J., Schmidt, A., Easter, R., Solomon, S., Kinnison, D. E., Ghan, S. J., Neely, R. R., Marsh, D. R., Conley, A., Bardeen, C. G., and Gettelman, A.: Global volcanic aerosol properties derived from emissions, 1990–2014, using CESM1(WACCM), J Geophys Res, 121, https://doi.org/10.1002/2015JD024290, 2016.

Morgenstern, O., Braesicke, P., O'Connor, F. M., Bushell, A. C., Johnson, C. E., Osprey, S. M., and Pyle, J. A.: Evaluation of the new UKCA climate-composition model – Part 1: The stratosphere, Geosci Model Dev, 2, 43–57, https://doi.org/10.5194/gmd-2-43-2009, 2009.

Morgenstern, O., O'Connor, F. M., Johnson, B. T., Zeng, G., Mulcahy, J. P., Williams, J., Teixeira, J., Michou, M., Nabat, P., Horowitz, L. W., Naik, V., Sentman, L. T., Deushi, M., Bauer, S. E., Tsigaridis, K., Shindell, D. T., and Kinnison, D. E.: Reappraisal of the Climate Impacts of Ozone-Depleting Substances, Geophys Res Lett, 47, e2020GL088295, https://doi.org/10.1029/2020GL088295, 2020.

Morgenstern, O., Frith, S. M., Bodeker, G. E., Fioletov, V., and van der A, R. J.: Reevaluation of Total-Column Ozone Trends and of the Effective Radiative Forcing of Ozone-Depleting Substances, Geophys Res Lett, 48, e2021GL095376, https://doi.org/10.1029/2021GL095376, 2021.

Myhre, G., Shindell, D., Bréon, F.-M., Collins, W., Fuglestvedt, J., Huang, J., Koch, D., Lamarque, J.-F., Lee, D., Mendoza, B., Nakajima, T., Robock, A., Stephens, G., Takemura, T., and Zhang, H.: Anthropogenic and Natural Radiative Forcing, in: Climate Change 2013: The Physical Science Basis. Contribution of Working Group I to the Fifth Assessment Report of the Intergovernmental Panel on Climate Change, edited by: Stocker, T. F., Qin, D., Plattner, G.-K., Tignor, M., Allen, S. K., Boschung, J., Nauels, A., Xia, Y., Bex, V., and Midgley, P. M., Cambridge University Press, Cambridge, United Kingdom and New York, NY, USA, 659–740, https://doi.org/10.1017/ CBO9781107415324.018, 2013.

Newman, P. A., Daniel, J. S., Waugh, D. W., and Nash, E. R.: A new formulation of equivalent effective stratospheric chlorine (EESC), Atmos Chem Phys, 7, 4537–4552, https://doi.org/10.5194/acp-7-4537-2007, 2007.

O'Connor, F. M., Johnson, B. T., Jamil, O., Andrews, T., Mulcahy, J. P., and Manners, J.: Apportionment of the Pre-Industrial to Present-Day Climate Forcing by Methane Using UKESM1: The Role of the Cloud Radiative Effect, J Adv Model Earth Syst, 14, e2022MS002991, https://doi.org/10.1029/2022MS002991, 2022.

Orbe, C., Rind, D., Jonas, J., Nazarenko, L., Faluvegi, G., Murray, L. T., Shindell, D. T., Tsigaridis, K., Zhou, T., Kelley, M., and Schmidt, G. A.: GISS Model E2.2: A Climate Model Optimized for the Middle Atmosphere—2. Validation of Large-Scale Transport and Evaluation of Climate Response, Journal of Geophysical Research: Atmospheres, 125, https://doi.org/10.1029/2020JD033151, 2020.

https://doi.org/10.5194/egusphere-2025-6033
Preprint. Discussion started: 15 January 2026

Prather, M. J., Holmes, C. D., and Hsu, J.: Reactive greenhouse gas scenarios: Systematic exploration of uncertainties and the role of atmospheric chemistry, Geophys Res Lett, https://doi.org/10.1029/2012GL051440, 2012.

Putman, W. M. and Lin, S. J.: Finite-volume transport on various cubed-sphere grids, J Comput Phys, 227, 55–78, https://doi.org/10.1016/J.JCP.2007.07.022, 2007.

Pyle, J. A., Keeble, J., Abraham, N. L., Chipperfield, M. P., and Griffiths, P. T.: Integrated ozone depletion as a metric for ozone recovery, Nature, 608, https://doi.org/10.1038/s41586-022-04968-8, 2022.

Ramaswamy, V.: "Radiative forcing of climate change". Climate Change 2001: The Scientific Basis, Cambridge, United Kingdom: Cambridge University Press, 2001.

Ramaswamy, V., Schwarzkopf, M. D., and Shine, K. P.: Radiative forcing of climate from halocarbon-induced global stratospheric ozone loss, Nature, 355, https://doi.org/10.1038/355810a0, 1992.

Sander, S. P., Friedl, R. R., Ravishankara, A. R., Kolb, C. E., Nasa, M. J. K., Washington, H., Molina, D. C. M. J., Moortgat, G. K., Keller-Rudek, H., Finlayson-Pitts, B. J., Wine, P. H., Huie, R. E., and Orkin, V. L.: Chemical Kinetics and Photochemical Data for Use in Atmospheric Studies Evaluation Number 15 NASA Panel for Data Evaluation, 2006.

Séférian, R., Nabat, P., Michou, M., Saint-Martin, D., Voldoire, A., Colin, J., Decharme, B., Delire, C., Berthet, S., Chevallier, M., Sénési, S., Franchisteguy, L., Vial, J., Mallet, M., Joetzjer, E., Geoffroy, O., Guérémy, J. -F., Moine, M. -P., Msadek, R., Ribes, A., Rocher, M., Roehrig, R., Salas-y-Mélia, D., Sanchez, E., Terray, L., Valcke, S., Waldman, R., Aumont, O., Bopp, L., Deshayes, J., Éthé, C., and Madec, G.: Evaluation of CNRM Earth-System model, CNRM-ESM 2-1: role of Earth system processes in present-day and future climate, J Adv Model Earth Syst, https://doi.org/10.1029/2019MS001791, 2019.

Sellar, A. A., Jones, C. G., Mulcahy, J. P., Tang, Y., Yool, A., Wiltshire, A., O'Connor, F. M., Stringer, M., Hill, R., Palmieri, J., Woodward, S., de Mora, L., Kuhlbrodt, T., Rumbold, S. T., Kelley, D. I., Ellis, R., Johnson, C. E., Walton, J., Abraham, N. L., Andrews, M. B., Andrews, T., Archibald, A. T., Berthou, S., Burke, E., Blockley, E., Carslaw, K., Dalvi, M., Edwards, J., Folberth, G. A., Gedney, N., Griffiths, P. T., Harper, A. B., Hendry, M. A., Hewitt, A. J., Johnson, B., Jones, A., Jones, C. D., Keeble, J., Liddicoat, S., Morgenstern, O., Parker, R. J., Predoi, V., Robertson, E., Siahaan, A., Smith, R. S., Swaminathan, R., Woodhouse, M. T., Zeng, G., and Zerroukat, M.: UKESM1: Description and Evaluation of the U.K. Earth System Model, J Adv Model Earth Syst, 11, 4513–4558, https://doi.org/10.1029/2019MS001739, 2019.

Shindell, D., Faluvegi, G., Nazarenko, L., Bowman, K., Lamarque, J. F., Voulgarakis, A., Schmidt, G. A., Pechony, O., and Ruedy, R.: Attribution of historical ozone forcing to anthropogenic emissions, Nat Clim Chang, 3, https://doi.org/10.1038/nclimate1835, 2013a.

Shindell, D. T., Pechony, O., Voulgarakis, A., Faluvegi, G., Nazarenko, L., Lamarque, J.-F., Bowman, K., Milly, G., Kovari, B., Ruedy, R., and Schmidt, G. A.: Interactive ozone and methane chemistry in GISS-E2 historical and future climate simulations, Atmos Chem Phys, 13, 2653–2689, https://doi.org/10.5194/acp-13-2653-2013, 2013b.

https://doi.org/10.5194/egusphere-2025-6033
Preprint. Discussion started: 15 January 2026

Skeie, R. B., Myhre, G., Hodnebrog, Ø., Cameron-Smith, P. J., Deushi, M., Hegglin, M. I., Horowitz, L. W., Kramer, R. J., Michou, M., Mills, M. J., Olivié, D. J. L., Connor, F. M. O., Paynter, D., Samset, B. H., Sellar, A., Shindell, D., Takemura, T., Tilmes, S., and Wu, T.: Historical total ozone radiative forcing derived from CMIP6 simulations, NPJ Clim Atmos Sci, 3, 32, https://doi.org/10.1038/s41612-020-00131-0, 2020.

Solomon, S., Kinnison, D., Bandoro, J., and Garcia, R.: Simulation of polar ozone depletion: An update, J Geophys Res, 120, https://doi.org/10.1002/2015JD023365, 2015.

Szopa, S., Naik, V., Berntsen, T., Collins, W. D., Fuzzi, S., Gallardo, L., Kiendler-Scharr, A., Klimont, Z., Liao, H., Unger, N., and Zanis, P.: Short-lived Climate Forcers, in: Climate Change 2021: The Physical Science Basis. Contribution of Working Group I to the Sixth Assessment Report of the Intergovernmental Panel on Climate Change, edited by: Masson-Delmotte, V., Zhai, P., Connors, S. L., Pean, C., Berger, S., Caud, N., Chen, Y., Goldfarb, L., Gomis, M. I., Huang, M., Leitzell, K., Lonnoy, E., Matthews, J. B. R., Maycock, T. K., Waterfield, T., Yelekci, O., Yu, R., and Zhou B, Cambridge University Press, Cambridge, United Kingdom and New York, NY, USA, 817–922, 2021.

Thomason, L. W., Ernest, N., Millán, L., Rieger, L., Bourassa, A., Vernier, J.-P., Manney, G., Luo, B., Arfeuille, F., and Peter, T.: A global space-based stratospheric aerosol climatology: 1979–2016, Earth Syst Sci Data, 10, 469–492, https://doi.org/10.5194/essd-10-469-2018, 2018.

Thornhill, G. D., Collins, W., Olivié, D., Skeie, R. B., Archibald, A., Bauer, S., Checa-Garcia, R., Fiedler, S., Folberth, G., Gjermundsen, A., Horowitz, L., Lamarque, J.-F., Michou, M., Mulcahy, J., Nabat, P., Naik, V., O'Connor, F. M., Paulot, F., Schulz, M., Scott, C. E., Séférian, R., Smith, C., Takemura, T., Tilmes, S., Tsigaridis, K., and Weber, J.: Climate-driven chemistry and aerosol feedbacks in CMIP6 Earth system models, Atmos Chem Phys, 21, 1105–1126, https://doi.org/10.5194/acp-21-1105-2021, 2021a.

Thornhill, G. D., Collins, W. J., Kramer, R. J., Olivié, D., Skeie, R. B., O'Connor, F. M., Abraham, N. L., Checa-Garcia, R., Bauer, S. E., Deushi, M., Emmons, L. K., Forster, P. M., Horowitz, L. W., Johnson, B., Keeble, J., Lamarque, J.-F., Michou, M., Mills, M. J., Mulcahy, J. P., Myhre, G., Nabat, P., Naik, V., Oshima, N., Schulz, M., Smith, C. J., Takemura, T., Tilmes, S., Wu, T., Zeng, G., and Zhang, J.: Effective radiative forcing from emissions of reactive gases and aerosols – a multi-model comparison, Atmos Chem Phys, 21, 853–874, https://doi.org/10.5194/acp-21-853-2021, 2021b.

Thornhill, G. D., Smith, L. A., and Shine, K. P.: Radiative Forcing From Halogen Reservoir and Halocarbon Breakdown Products, Journal of Geophysical Research: Atmospheres, 129, e2024JD040912, https://doi.org/10.1029/2024JD040912, 2024.

Tilmes, S., Hodzic, A., Emmons, L. K., Mills, M. J., Gettelman, A., Kinnison, D. E., Park, M., Lamarque, J. -F., Vitt, F., Shrivastava, M., Campuzano-Jost, P., Jimenez, J. L., and Liu, X.: Climate Forcing and Trends of Organic Aerosols in the Community Earth System Model (CESM2), J Adv Model Earth Syst, 2019MS001827, https://doi.org/10.1029/2019MS001827, 2019.

https://doi.org/10.5194/egusphere-2025-6033
Preprint. Discussion started: 15 January 2026

Toumi, R., Bekki, S., and Law, K. S.: Indirect influence of ozone depletion on climate forcing by clouds, Nature, 372, https://doi.org/10.1038/372348a0, 1994.

Velders, G. J. M., Andersen, S. O., Daniel, J. S., Fahey, D. W., and McFarland, M.: The importance of the Montreal Protocol in protecting climate, Proceedings of the National Academy of Sciences, 104, 4814–4819, https://doi.org/10.1073/PNAS.0610328104, 2007.

Volk, C. M., Elkins, J. W., Fahey, D. W., Dutton, G. S., Gilligan, J. M., Loewenstein, M., Podolske, J. R., Chan, K. R., and Gunson, M. R.: Evaluation of source gas lifetimes from stratospheric observations, Journal of Geophysical Research Atmospheres, 102, 25543–25564, https://doi.org/10.1029/97JD02215, 1997.

Western, L. M., Shine, K. P., and Collins, W. J.: The Net Radiative Forcing from Ozone-Depleting Substances and its Uncertainty, In Review Geophys. Res. Lett.

WMO: Scientific Assessment of Ozone Depletion: 2022, GAW Report No. 278, Geneva, 509 pp., 2022.

Yukimoto, S., Kawai, H., Koshiro, T., Oshima, N., Yoshida, K., Urakawa, S., Tsujino, H., Deushi, M., Tanaka, T., Hosaka, M., Yabu, S., Yoshimura, H., Shindo, E., Mizuta, R., Obata, A., Adachi, Y., and Ishii, M.: The meteorological research institute Earth system model version 2.0, MRI-ESM2.0: Description and basic evaluation of the physical component, Journal of the Meteorological Society of Japan, 97, https://doi.org/10.2151/jmsj.2019-051, 2019.